A Computational and Spectroscopic Study of the Electronic Structure of V 2 O 5 -Based Cathode Materials

Evgenii Roginskii, Mikhail Smirnov, Konstantin Smirnov, Rita Baddour-Hadjean, Jean Pierre Pereira-Ramos, Alexander Smirnov, Valery Yu. Davydov

A Computational and Spectroscopic Study of Electronic Structure of V_2O_5-based Cathode Materials

Evgenii M. Roginskii,[*,†] Mikhail B. Smirnov,[‡] Konstantin S. Smirnov,[*,¶] Rita Baddour-Hadjean,[§] Jean-Pierre Pereira-Ramos,[§] Alexander N. Smirnov,[†] and Valery Yu. Davydov[†]

[1]

†*Ioffe Institute, Polytekhnicheskaya 26, 194021 St. Petersburg, Russia*

‡*Faculty of Physics, St. Petersburg State University, Petrodvoretz, 194508 St. Petersburg, Russia*

¶*Univ. Lille, CNRS, UMR 8516 – LASIRe – Laboratoire Avancé de Spectroscopie pour les Interactions la Réactivité et l'Environnement, F-59000 Lille, France*

§*Institut de Chimie et des Matériaux Paris-Est (ICMPE), UMR 7182 CNRS et Université Paris-Est Créteil, 2 rue Henri Dunant, 94320 Thiais, France*

E-mail: e.roginskii@mail.ioffe.ru; konstantin.smirnov@univ-lille.fr

Abstract

The electronic structure of α-V_2O_5, γ'-V_2O_5 and γ-MeV_2O_5 (Me = Li, Na) bronzes is studied by quantum-chemical calculations completed by spectroscopic experiments. The calculations are performed using G_0W_0 method with DFT+U self-consistent wave-function as an initial approximation. The electronic band gap $E_g = 2.89$ eV calculated for α-V_2O_5 is found to be in a fair agreement with available experimental data. The strategy was then applied to studying the electronic structure of the γ'-V_2O_5 phase and γ-MeV_2O_5 bronzes for which no experimental band gap data exist in the literature. Computed E_g values are equal to 3.17 eV, 1.21 eV and 1.18 eV for γ'-V_2O_5, γ-LiV_2O_5 and γ-NaV_2O_5, respectively. The nature of alkali metal atom is obtained to have little influence on the structure and electronic states of the bronzes. Raman spectra recorded with different wavelengths of exciting radiation have allowed the determination of energy threshold corresponding to the transition from off-resonance to resonance Raman scattering process. In this way, a band gap value in the range 2.54 – 2.71 eV for α-V_2O_5 and γ'-V_2O_5 is obtained in a good agreement with the experimental values for the α-phase. Raman spectra of γ-MeV_2O_5 suggest the band gap smaller than 1.58 eV in these materials, whereas the photoluminescence measurements yield $E_g \approx 0.95$ eV for the γ-LiV_2O_5 bronze. Remarkably, the result of the G_0W_0 calculations lies in between the experimental estimates. Strong similarity of structures and electronic states of γ-LiV_2O_5 and γ-NaV_2O_5 accounts for their the same operating voltage when used as cathodes in Li(Na)-ion batteries.

Introduction

The rich chemistry and polymorphism of vanadium pentoxide (V_2O_5) have made this material very interesting for fundamental research and for many applications in heterogeneous catalysis,[1] electrochromism[2] and electrochemical energy storage.[3] Vanadium pentoxide is a typical intercalation compound because of its layered structure. This structural peculiarity is illustrated in Figure 1 for the α-V_2O_5 and γ'-V_2O_5 phases which are the main objects of the present work. These structures exhibit characteristics typical of all V_2O_5 polymorphs, *i.e.* V_2O_5 chains running in the b crystallographic direction and connected in layers *via* V-O2 "ladder" steps; the layers are then stacked in the third dimension and held together by weak interlayer interactions. Puckering layers in the γ'-V_2O_5 lattice compared to flat layers in the α-V_2O_5 structure results in the c lattice parameter of the γ'-V_2O_5 unit cell being approximately twice of the parameter of α-V_2O_5 one.

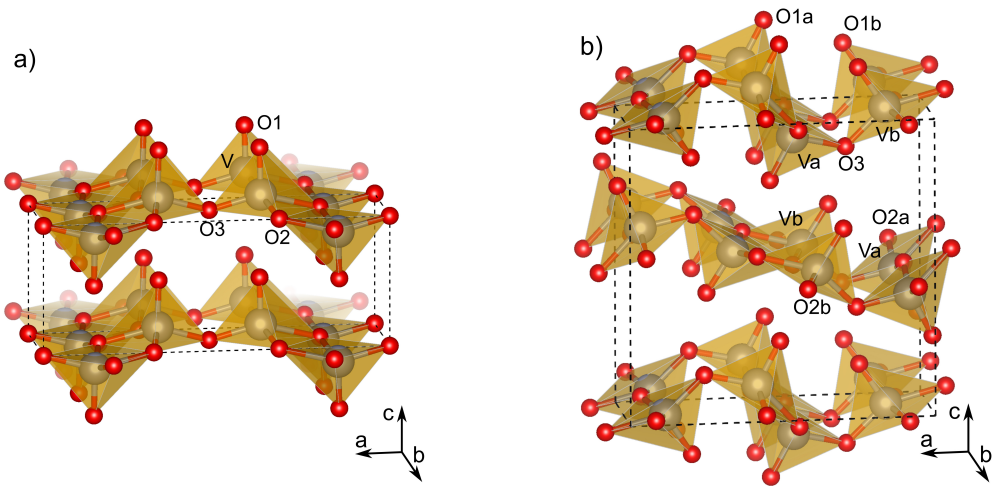

Figure 1: Structures of α-V_2O_5 (a) and γ'-V_2O_5 (b). The crystallographic unit cells are shown by dashed lines; atom labels correspond to those used throughout the paper.

Very early, the α-form (Figure 1a) has been identified as a promising cathode material for secondary lithium batteries.[3–5] Functioning of the batteries relies on the electron transfer reaction accompanied by the electrochemical intercalation/de-intercalation of alkali metal atoms into the oxide structure. The insertion of alkali metal (Me) in the interlayer space

of V_2O_5 lattice leads to vanadium oxide bronzes with general formula $Me_xV_2O_5$ showing remarkable versatility as a function of the nature of intercalated alkali atom.[6] The presence of two V^{5+} ions per V_2O_5 unit allows to reach a high storage capacity that can amount to 300 mAh g^{-1} corresponding to the reversible accommodation of two lithium ions/mole in the 2.3–3.5 V potential window.[3,5] The interest of the γ'-V_2O_5 polymorph (Figure 1b) for the electrochemical applications has been recently demonstrated in the case of lithium[7,8] and sodium insertion.[9,10] A higher open circuit voltage combined with lower diffusion barriers afford superior electrochemical properties to this material compared to the α-V_2O_5 form.[8,10] A readily accessible V^{5+}/V^{4+} redox couple and the stability of different local coordination environments of the vanadium atoms (octahedral, distorted octahedral, square pyramid, ...), result in the flexibility of the layered V_2O_5 structures and in their ability to accommodate point defects through a crystallographic shear and/or charge localization/delocalization.[11] The lattice of γ-MeV_2O_5 bronzes (Me = Li, Na) is very close to that of γ'-V_2O_5 shown in Figure 1b and in what follows, we therefore use the same notation for the atoms V and O atoms in both the pure and intercalated structures.

The electronic structure and the energy difference between the top of the valence band and the bottom of the conduction band, the band gap E_g, are fundamental characteristics of material that determine its electric conductivity and optical properties. The conductivity is directly related to the concentration of charge carriers that, in its turn, depends on the band gap, and impacts high rate capabilities of electrode materials.[12] The band gap is also an important factor in electrochemical applications, in particular for designing an electrode–electrolyte pair.[13,14] Among different structural modifications of vanadium pentoxide, a value of the band gap has been measured only for the α-V_2O_5 polymorph,[15–17] while no such data exist for γ-$Me_xV_2O_5$ bronzes which, as it was mentioned above, have more promising properties for the usage as cathode material for Me-ion batteries.[9,10,18]

Nowadays, the lack of experimental data can in part be compensated by the use of atomistic simulations that have become a valuable and reliable tool in materials research.

Most of electronic-structure calculations of materials employs methods based on the density functional theory (DFT). However, a correct description of electronic structure with DFT encounters problems due to the energy derivative discontinuity and the local character of exchange-correlation (XC) functionals of commonly used local density approximation (LDA) and generalized gradient approximation (GGA) to DFT. The derivative discontinuity makes the band gap to be known up to a constant,[19] while the local character of LDA and GGA XC functionals causes artifacts in the calculations for materials with occupied d and f states,[20] such as transition metal oxides. To overcome the shortcomings, computational investigations of the electronic structure of solids often rely on the DFT+U approach, that introduces an on-site repulsion for localized electrons.[21] Alternatively, the local character of the LDA and GGA XC functionals is remedied in hybrid functionals, such as PBE0[22] and HSE06[23,24], that bring a non-local exchange energy of Hartee-Fock (HF) theory into DFT. While these approaches generally improve results for the electronic structure of materials, they introduce empirical parameters (Hubbard parameter U in DFT+U and the portion of HF exchange in hybrid functionals) that may not work properly outside the range of systems (properties) to which they are fitted.

In order to sidestep the deficiencies inherent to DFT, one can employ computations that use a GW approximation based on the many-body perturbation theory. The GW calculations permit a more accurate description of the electronic states in a systems of interacting electrons and nuclei,[25,26] but at the expense of being much more computationally expensive than their DFT counterparts, especially if the self-consistent solution is sought. Although the GW method provides results in a good agreement with experimental data, it was found that the computations overestimate the band gap if the Green's function G and the screened Coulomb interaction matrix W are updated until a self-consistency. On the other hand, a "single-shot" G_0W_0 calculations including of one iteration step underestimate experimental values. A compromise was found in the case when only the Green's function is updated until the self-consistency, while the screened Coulomb potential is kept unchanged

(GW_0 approximation).[25] Nevertheless, even GW_0 remains computationally demanding for systems with dozens of atoms in the unit cell. Bruneval and Marques[27] reported on results of G_0W_0 calculations starting from electronic states obtained by different methods. The authors found that the accuracy of the calculations could be improved by using a solution obtained with a hybrid XC functional as an initial approximation. Alternatively, Scheffler and co-workers have shown that the use of LDA+U solution in G_0W_0 method provides an accurate description of electronic structure in systems with occupied d- or f-electron shells.[28,29]

The structure, lattice dynamics and electronic states of the α-phase of vanadium pentoxide have been studied with DFT methods in a number of works.[30–37] In order the calculations to correctly reproduce the layered structure of the material, the use of semi-empirical dispersion correction was found to be indispensable.[35,36] Band gap values computed in ref 30–32,34 were obtained to be smaller than the experimental data[15–17] and the agreement with the experiment could be improved by the inclusion of on-site Hubbard term penalizing the electron delocalization into the Hamiltonian.[34] Like the experimental research, computational DFT studies of other V_2O_5 structures paid little attention to their electronic states.[32,37–39] Investigations of V_2O_5 materials with the GW methods are scarce. The electronic structure of α-V_2O_5 was investigated in self-consistent GW calculations by Bhandari and Lambrecht.[40] In line with aforementioned results, the authors obtained the band gap significantly larger than the experimental values.[15–17] The discrepancy was explained as a result of enhanced screening of the Coulomb potential due to an increase of the static dielectric constant because of large LO-TO splitting in the system. To the best of our knowledge, no other attempts of exploring V_2O_5-based materials with GW methods were undertaken.

The present work reports on a combined computational and experimental study of the electronic structure, particulary the band gap, of pure α-V_2O_5, γ'-V_2O_5 and of alkali-atom intercalated γ-MeV_2O_5 (Me = Li, Na) materials. The computations have adopted a strategy in which the electronic structure of α-V_2O_5 was investigated by G_0W_0 method with the self-

consistent LDA+U solution as an initial approximation to the many-particle wavefunction.[29] To avoid the arbitrariness in the choice of Hubbard parameter, value of U was obtained using density functional perturbation theory.[41] A good agreement of the calculated band gap value with the available experimental data for this structure enabled us to extend the strategy to the computation of the electronic structure of γ'-V_2O_5 and of the MeV_2O_5 bronzes. In the absence of any experimental information on the band gap in these materials, Raman and photoluminescence experiments performed with different wavelengths of the exciting radiation provided experimental estimates for E_g and validated results of the electronic-structure calculations.

Methods

Experimental procedure and materials characterisation

α-V_2O_5 was prepared through the polyol method described in ref 42. Chemical lithiation of α-V_2O_5 was performed under mild conditions, using lithium iodide in excess (molar ratio 2:1) to obtain the δ-LiV_2O_5 precursor that transforms to γ-LiV_2O_5 when heat-treated at 300°C.[43] γ'-V_2O_5 is obtained by chemical oxidation of γ-LiV_2O_5 using NO_2BF_4 in molar excess (2:1), as described in ref 18. γ-NaV_2O_5 is come by chemical sodiation of γ'-V_2O_5 using anhydrous sodium iodide (molar excess 2:1).[11] The synthesis procedure results in a change of samples color from orange for the pure V_2O_5 phases to dark green (nearly black) for the alkali-atom intercalated compounds. The structural parameters of α-V_2O_5, γ'-V_2O_5 γ-LiV_2O_5 γ-NaV_2O_5 are summarized in Table S1 of Supporting Information (SI). The experimental Raman spectra of the materials are plotted in Figure S1 of SI, while the assignment of spectral features in the spectra is discussed in detail elsewhere.[18,39,44–46]

The Raman measurements of α-V_2O_5 and γ'-V_2O_5 were performed at room temperature using LaBRAM HR 800 (Jobin-Yvon-Horiba) micro-Raman spectrometer equipped with a back illuminated charge coupled device detector (Spex CCD) cooled by Peltier effect to

200 K. In the measurements, the exciting light at four wavelengths was used, namely: He-Ne laser (λ= 632.8 nm), and tunable Ar+ laser (λ = 514, 488 and 458 nm). A 100× LWD objective was used to focus the laser light to a spot size of 1 μm^2 on the sample surface. To avoid a local heating of the sample, the power of the laser beam was adjusted to 0.2–0.5 mW with neutral filters of various optical densities. The Raman and photoluminescence measurements of γ-LiV_2O_5 were performed with a T64000 (Horiba Jobin-Yvon) spectrometer equipped with a confocal microscope and a silicon CCD detector cooled by liquid nitrogen. Room temperature Raman spectra were excited by a 442 nm HeCd laser line, 532 nm line of a Nd:YAG laser (Torus, Laser Quantum, Inc.), and λ_0 = 785 nm line of nearinfrared laser diode (TEC, Thorlabs Inc.). Photoluminescence spectra were excited by λ_0 = 785 nm (TEC, Thorlabs Inc.) and λ_0 = 244 nm (Coherent Innova 300C MotoFreD Ion Laser). The measurements in the temperature range from 78 to 300 K were carried out in a temperature controlled microscope stage Linkam THMS600. All spectra were measured in a backscattering geometry.

Computational procedure

The *ab initio* calculations presented in the paper were carried out with ABINIT software package.[47,48] The LDA calculations employed the pseudopotential method and the plane wave basis set for valence electronic states, and used the PW exchange-correlation functional.[49] The interactions between the core and valence electrons were described with the projector-augmented wave (PAW) method.[50,51] The $3p3d4s$ states of V atom, $2s2p$ states of O atom and $2s2p3s$ states of sodium were considered as valence states; the Li atom was treated at the all-electron level. In order to take into account the reduction of the transition metal upon the intercalation of alkali atoms, spin-polarized calculations were performed. The localized character of the $3d$ states of V atoms was taken into consideration via the Hubbard term in the Hamiltonian (DFT+U method).[21] Choice of the Hubbard parameter U is discussed below in detail.

For each system studied the equilibrium structure was obtained in the following way. First, the geometry optimization of the unit cell was performed for a series of five volumes. In these calculations, both atomic positions and lattice parameters were allowed to vary, whereas the volume and the symmetry of the crystalline lattice were kept fixed. The Kohn-Sham equations were solved iteratively with a stopping criterion 10^{-12} Ha for the energy convergence and the geometry optimization was considered to be completed if the maximum force on ions was less than 5×10^{-5} Ha/Bohr. The obtained energy *vs.* volume dependence was fitted by the Murnaghan equation of state[52] that provided an equilibrium cell volume. Then, the volume was used in a final optimization run that produced the equilibrium lattice parameters and atomic coordinates. This approach permitted to avoid problems related to the Pulay stress and to the variation of size of plane wave basis set that accompany calculations with simultaneous optimization of both the volume and atomic positions. The total energy was tested for the convergence with respect to the k-point grid and number of plane waves, the latter is controlled by a plane wave kinetic energy cutoff. It was found that the convergence of the total energy within 10^{-4} Ha/atom was achieved with the energy cutoff of 40 Ha and $2 \times 6 \times 6$ grids and $2 \times 6 \times 2$ grids of k-points chosen according to the Monkhorst-Pack scheme [53] in the irreducible part of the Brillouin zone (BZ) of the α-V_2O_5, and γ'-V_2O_5 and γ-MeV_2O_5 structures, respectively. The so-obtained equilibrium structures were employed in subsequent calculations that used the above calculation parameters and the convergence criterion. The LDA+U calculations were performed considering a partial occupation of electronic states with a gaussian smearing of 1 mHa width.

The quasi-particle GW calculations[54] used the frequency dependence of the screened Coulomb interaction obtained within the random-phase approximation by the contour deformation method.[55] The exchange and correlation components of the self-energy were computed using the plane wave basis set with the energy cutoffs of 40 Ha and 10 Ha, respectively. The calculation of the polarizability and Green's function employed 268 unoccupied states in the conduction band. The BZ integration was performed over the $2 \times 4 \times 4$ and $2 \times 4 \times 2$ grid

for α-V_2O_5 and for γ'-V_2O_5 and γ-MeV_2O_5, respectively. The initial single-particle Green's function G_0 and the screened Coulomb potential W_0 were constructed using the LDA+U eigenstates and eigenvalues, that is known as G_0W_0@LDA+U approach.[28,29,56] In order to exclude double-counting term contained in the LDA+U eigenvalues,[57] the quasi-particle energies $\mathcal{E}^{\sigma}_{n\mathbf{k}}$ were calculated using following expression:[29]

$$\mathcal{E}^{\sigma}_{n\mathbf{k}} = \bar{\epsilon}^{\sigma}_{n\mathbf{k}} + Z_{n\mathbf{k}}(\bar{\epsilon}^{\sigma}_{n\mathbf{k}}) \left[\Sigma^{\sigma}_{n\mathbf{k}}(\bar{\epsilon}^{\sigma}_{n\mathbf{k}}) - (\nu_{xc})^{\sigma}_{n\mathbf{k}}\right], \tag{1}$$

where σ is the spin index (up/down), $\mathbf{k}$ – wavevector, $\bar{\epsilon}^{\sigma}_{nk}$ – single-particle energies calculated with LDA+U wave functions, Z_{nk} – renormalization factor, and ν_{xc} – Kohn-Sham (KS) exchange-correlation operator. The band structure in the GW calculations was obtained from the KS band structure by applying the energy-dependent scissors operator generated by a fit of GW-KS energy differences over a dense grid of k-points as a function of the KS eigenvalues.[58,59]

Results and discussion

Choice of Hubbard parameter U. The use of the LDA+U solution in the GW calculations requires the knowledge of the Hubbard parameter U. Previous DFT calculation of V_2O_5 bronzes[34,39] made use of $U = 4$ eV that was obtained from comparison of computed band gap to E_g values measured by the X-ray and UV photoelectron spectroscopies.[60,61] However, this value of U could not be simply transferred to the present calculations. In fact, the used DFT+U approach relies on two Hubbard parameters U and J which being combined give an effective parameter $U_{eff} = U - J$ and it is U_{eff} that corresponds to U in ref 34,39. Making use of the linear response method,[41,62,63] we have computed $U = 4.5$ eV and $U = 4.9$ eV for the α-V_2O_5 and γ'-V_2O_5 structures, respectively. For the alkali atom intercalated γ-MeV_2O_5 compound the method has yielded an U value of 5.2 eV. Constrained DFT calculations of U and J for several transition metal oxides have given $U \approx 5$ eV and

$J \approx 1$ eV[29] that results in $U_{eff} \approx 4$ eV. In our choice of J we have relied on an estimation $J \approx 0.1\,U$ that can be proposed considering the explicit formulas for these quantities.[21,37] Given the likeness of the results obtained by the linear response method and the outcome of the previous calculations,[29] we have chosen to use $U = 4.5$ eV and $J = 0.5$ eV for all the systems in the study without adjustment.

The comparison of electron density of states (DOS) obtained for γ-LiV_2O_5 with these values of U and J to DOS computed in ref 39 shows their a good agreement (see Figure S2). Futhermore, auxiliary calculations have revealed a small difference between the target quantities computed with the system-specific (obtained with the linear response method) and the generic U and J parameters (Table S3). A weak dependence of the electronic structure on the parameter values indicate that their values are "physically" meaningful.[29]

Electronic structure and Raman spectra of pure V_2O_5 structures. The geometry optimization of the pristine V_2O_5 structures at the LDA+U level does not notably improve the agreement between the computed and experimental structural characteristics in comparison to the conventional LDA calculations (Table S1). The result is perfectly understandable because none of the $3d$ states of vanadium atoms, which are subjected to the Hubbard term, is occupied in these systems. However, the use of U in the LDA calculations pushes the bottom of the conduction band up, thus increasing the electronic band gap E_g. The direct band gap E_g^d for the α-V_2O_5 structure computed at the LDA+U level is equal to 1.79 eV, 1.84 eV and 1.87 eV for $U_{eff} = 0$ eV, $U_{eff} = 2.7$ eV and $U_{eff} = 4$ eV, respectively. The optical absorption measurements on α-V_2O_5 monocrystals have given $E_g = 2.35 \pm 0.01$ eV[15] and $E_g = 2.31 \pm 0.01$ eV[16] and the band gap at $T = 0$ K estimated by extrapolating these experimental data is 2.49 eV to 2.54 eV.[16] More recent photoemission spectroscopic experiments reported the band gap of 2.8 eV for this material.[17] Although the LDA+U slightly increases E_g value, the band gap still remains markedly smaller than the experimental conterparts and the energy derivative discontinuity makes the quantity known up to a constant.[19] As it

was mentioned in Introduction, one may expect to solve the problem, at least in part, by using the GW method while a high computational cost of such calculations can be reduced by taking the self-consistent LDA+U solution as an initial approximation.[56]

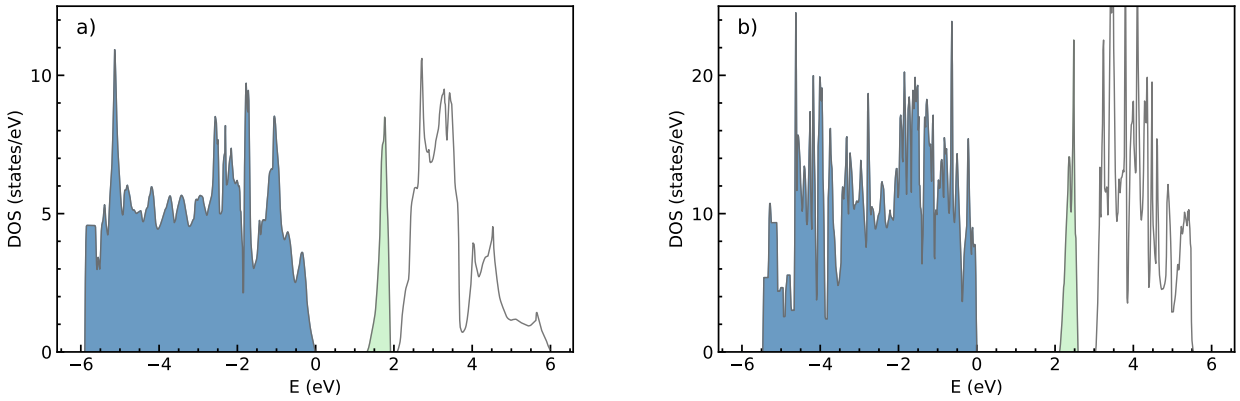

Figure 2: Densities of states (DOS) for α-V_2O_5 (a) and γ'-V_2O_5 obtained in the LDA+U calculations. The density of states in valence band and in the V^{3d} conduction band discussed in the text are shaded by the blue and light green color, respectively. The origin of the energy axis is placed at the Fermi energy.

Density of electronic states (DOS) for α-V_2O_5 computed at the LDA+U level is presented in Figure 2a while the partial DOS (PDOS) can be found in Figure S3. The first conduction band with lowest energy appears as a sharp peak in DOS (shaded with light green color in Figure 2). The nature of states in the band is important for understanding the change of the electronic structure upon the intercalation of alkali metal atoms. As it has been found previously, the conduction band is dominanted by d-states of vanadium atoms[32,40] and this conclusion is confirmed by the analysis of PDOS (Figure S3). Since these V^{3d} states are unoccupied, the vanadium atoms are in the 5+ oxidation state in the pure compound. Such a band of localized V^{3d} states is typical for vanadium oxides including γ-V_2O_5 (Figure 2b)[64]. Anticipating the following discussion, the intercalation of alkali metal atoms injects additional electrons into the system that fill the states thus making the band valence and radically decreasing the band gap in the material.

Figure 3a presentss the band structure of α-V_2O_5 obtained in an "one-shot" G_0W_0@LDA+U calculation. The top of the valence band and the bottom of the conduction band are in the

vicinity of the T-point $(0, \frac{1}{2}, \frac{1}{2})$ and in the Γ-point of the BZ, respectively. The direct gap E_g^d is equal to 2.89 eV and corresponds to the transition in the $(0, \frac{1}{4}, \frac{1}{2})$ point of the BZ, the indirect band gap E_g^i amounts to 2.42 eV. The computed E_g^d value is slightly greater than the estimation of $2.49 - 2.54$ eV at $T = 0$ K obtained from the UV-vis adsorption data,[15,16] while it is close to an estimate $2.98 - 3.01$ eV at $T = 0$ K found by extrapolating the band gap measured in the photoemission experiments.[17] Our trial calculations have shown that a small variation of U_{eff} does not significantly influence the values of the band gap and therefore, the choice of $U_{eff} = 4$ eV seems to be reasonable.

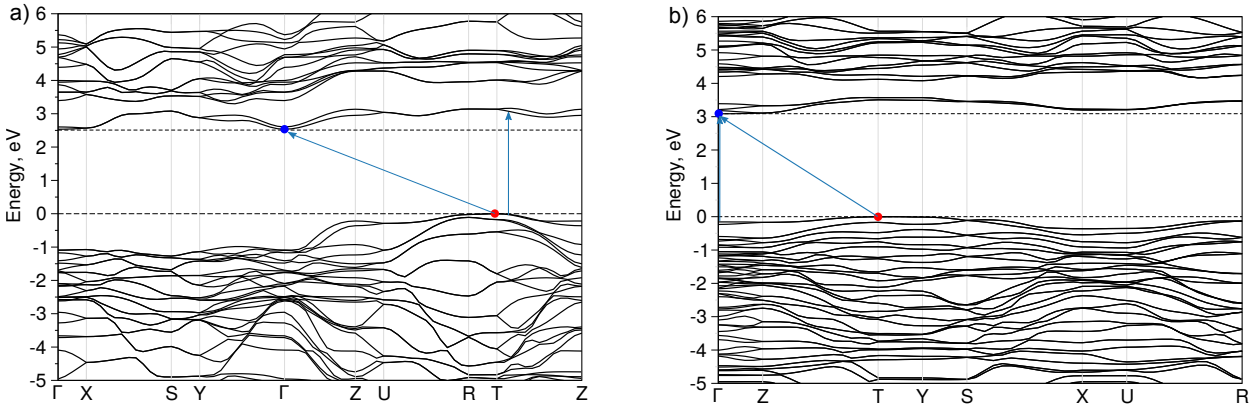

Figure 3: Electronic band structure of α-V_2O_5 (a) and γ'-V_2O_5 (b) calculated in G_0W_0@LDA+U approximation; dashed lines indicate the positions of the Fermi level and the bottom of the conduction band. The bottom of conduction band and the top of the valence band pointed out by blue and red dots, respectively. Direct and indirect interband transitions are respectively shown by vertical and oblique arrows. The origin of energy axis is placed at E_F (Fermi energy).

Previous self-consistent GW calculations[40] of α-V_2O_5 have given band gap values $E_g^d = 4.8$ eV and $E_g^i = 4$ eV that significantly exceed the experimental data.[15–17] The overestimation has been explained as a consequence of large LO-TO splitting that reduces screened Coulomb interaction in this polar material thus, increasing the gap. Due to the presence of the integrable singularity of Coulomb potential at the Γ-point, which hinders the convergence with respect to the number of k-points used to sample the BZ, the bare Coulomb potential in the present calculations was replaced by an auxiliary function[65] within a sphere of radius 150 Bohr that has resulted in the convergence of exact exchange energy better than 5×10^{-4} Ha.

The results presented above show that the use of this approach and of a DFT solution as the input to the G_0W_0 calculations, gives the band gap in the α-V_2O_5 in a much better agreement with the experimental data than the E_g values obtained in the self-consistent GW calculations.[40]

The electronic band structure obtained for γ'-V_2O_5 in a G_0W_0@LDA+U calculation using the above approach is presented in Figure 3b. The top of the valence band and the bottom of the conduction band are found in the vicinity of the T-point (0, $\frac{1}{2}$, $\frac{1}{2}$) and in the Γ-point (0, 0, 0) of the BZ, respectively. The calculation yields the direct and indirect band gaps of 3.17 eV and 3.09 eV, respectively, and the direct gap corresponds to the transition in the Γ-point of the BZ. G_0W_0@LDA+U calculations using the U value obtained by linear response method has given slightly lower E_g values, namely 3.12 eV and 3.04 eV for the direct and indirect band gap, respectively (Table S3). To the best of our knowledge, no experimental data exist on the band gap in the material. Previously, Willinger *et al.*[32] computed E_g of 1.70 eV in γ'-V_2O_5 by using the full potential linearized augmented plane waves method; the value $E_g = 1.75$ eV was obtained for α-V_2O_5 by the authors.

Table 1 collects experimental and theoretical band gap values for the α-V_2O_5 and γ'-V_2O_5 materials. Comparison of the E_g values computed at different levels of theory shows that the use of the DFT+U approach yields a better agreement with the experimental data, in line with the outcome of previous studies[34]. Computations with the hybrid PBE0 functional using both the LCAO basis set[64] and plane waves (this work) strongly overestimate the band gap in the α phase. The HSE06 functional performs better, yet the band gap in the material is markedly greater than the experimental values. A better agreement with the experiment has been obtained at the GGA+U level in ref 34 that is not surprising as U in that study has been fitted to reproduce the experimental band gap. Despite a relatively high computational cost, the G_0W_0 calculation using LDA+U solution gives a very good estimation of E_g obtained in a purely *ab initio* way with the U parameter found with the linear response method[41].

Table 1: Experimental and calculated values of band gap E_g for the α-V_2O_5 and γ'-V_2O_5 polymorphs.

Polymorph	E_g (eV)	Method	Reference
α-V_2O_5	2.35 ± 0.01	Exp.[a], OA	15
	2.31 ± 0.01	Exp., OA	16
	2.8	Exp., PES	17
	1.74	Calc.[b], ASW/LDA	31
	1.6 (2.1)	Calc., PAW/GGA (GGA+U)	66
	1.38 (2.06)	Calc., PAW/LDA (PBE)	67
	1.92	Calc., PAW/PW91	68
	1.74	Calc., PAW/PBE	69
	2.26	Calc., PAW/PBE+U	34
	1.75	Calc., FPLAPW	32
	4.04	Calc., TZVP/PBE0	64
	4.83	Calc., SC GW	40
	1.79 (1.87)	Calc., PAW/LDA (LDA+U)	This work
	4.17	Calc., PW-NCPP/PBE0	This work
	3.43	Calc., PW-NCPP/HSE06	This work
	2.89	Calc., G_0W_0@LDA+U	This work
γ'-V_2O_5	1.70	Calc., FPLAPW	32
	4.23	Calc., TZVP/PBE0[e]	64
	1.93 (2.27)	Calc., PAW/LDA (LDA+U)	This work
	4.41	Calc., PW-NCPP/PBE0	This work
	3.64	Calc., PW-NCPP/HSE06	This work
	3.17	Calc., G_0W_0@LDA+U	This work

[a]Experiment: OA – optical absorption, PES – photoemission spectroscopy;
[b]Calculations: LDA, GGA - local density approximation and generalized gradient approximation to DFT, respectively; +U – inclusion of Hubbard term into Hamiltonian; PBE, PW91 – GGA exchange-correlation functionals; PBE0, HSE06 – hybrid HF-DFT functionals; ASW – augmented spherical wave; FPLAPW – full potential linearized augmented plane wave; SC GW – self-consistent GW approach; PAW – projector augmented wave; TZVP - polarization quality triple-zeta valence atomic basis set, PW-NCPP – plane wave basis set with norm-concerving pseudopotentials.

Besides the optical absorption or photoemission experiments, Raman spectroscopy can, in principle, provide information on the band gap value. Indeed, one can expect a notable change in the Raman spectrum of material as soon as the energy of exciting radiation exceeds E_g and thus, the scattering process occurs in the electron resonance conditions. Figure 4 displays Raman spectra of α-V_2O_5 and γ'-V_2O_5 samples measured with four different excitation wavelengths. One sees that all the spectra obtained with $\lambda_0 > 458$ nm are very similar to each other, whereas the spectra obtained with $\lambda_0 = 458$ nm strikingly differ from the spectra measured with excitation wavelengths of smaller energy. Despite a variation of shape of the most intense peak at *ca.* 500 cm^{-1}, the 458 nm spectra obtained from different spots on the sample's surface show a good reproducibility. Hence, such a dependence of the spectra on the excitation wavelength cannot be viewed as an artifact and the behavior allows us to suppose that the 458 nm spectra were measured in the electron resonance conditions. Then, it is reasonable to assume that the band gap value for the α-V_2O_5 and γ'-V_2O_5 materials at room temperature lies between 2.71 eV ($\lambda_0 = 458$ nm) and 2.54 eV ($\lambda_0 = 488$ nm). Making use of the relative band gap values in these materials obtained in the G_0W_0@LDA+U calculations, one can estimate the band gap in α-V_2O_5 to be slightly greater than 2.54 eV that well agrees with the previous experimental results.[16,17] The gap in γ'-V_2O_5 can then be evaluated to be slightly lesser than 2.71 eV that provides a first experimental estimation of this quantity for the material. It should be noted that the γ'-V_2O_5 sample was obtained by the chemical deintercalation of Li atoms from the γ-LiV_2O_5 bronze and, therefore its structure can contain a number of defects. Consequently, the above value likely underestimates the band gap in a defect-less structure of γ'-V_2O_5.

Figure 4 shows that the resonance Raman spectra of both the pure V_2O_5 structures are dominated by a peak at 500 cm^{-1}. According to our previous calculations,[39,44,46] the Raman features in this spectral region originate from vibrational modes involving stretching vibrations of V-O2 contacts in the ladder steps and of the bonds in the V-O3-V bridges[46] (see Figure 1b). The electronic-structure calculations indicate that the main contribution to

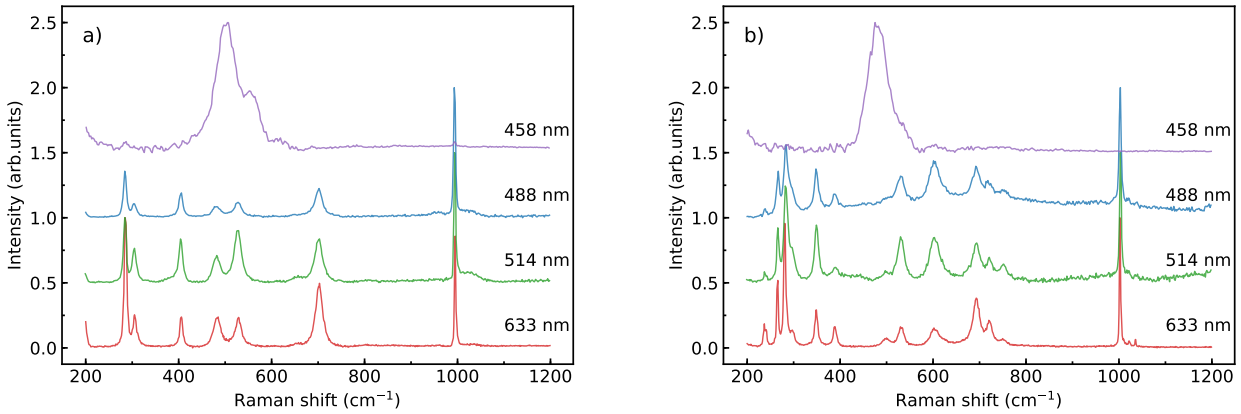

Figure 4: Raman spectra of α-V_2O_5 (a) and γ'-V_2O_5 (b) obtained with different wavelengths λ_0 of the incident radiation: $\lambda_0 = 633$ nm (red), $\lambda_0 = 514$ nm (green), $\lambda_0 = 488$ nm (blue), and $\lambda_0 = 458$ nm (violet).

the top of the valence band comes from the O2 and O3 oxygen atoms, whereas the bottom of the conduction band is formed by the d states of vanadiums. It is, therefore, not surprising that the Raman peaks due to vibrational modes involving displacements of these atoms are the most concerned by the electron resonance effect.

γ-MeV_2O_5 bronzes. In contrast to the pure V_2O_5 materials, a computational investigation of alkali atom intercalated MeV_2O_5 structures necessitates the use of theoretical approach that takes into account the localized character of partially occupied $3d$ vanadium states.[34,39] Figure 6 shows the G_0W_0@LDA+U electron band structure of γ-LiV_2O_5, the band structure of the γ-NaV_2O_5 bronze is very similar with a tiny difference in a value of the band gap (Figure S3). The electronic states at the Fermi level are formed by the d orbitals of Vb atoms occupied by electrons ejected from the outer s shell of the alkali metals, while the bottom of the conduction band is formed by the d orbitals of Va atoms, Figure 1b. From Figure 6 it follows that the γ-MeV_2O_5 bronzes are the direct transition semiconductors with the direct optical transition at the Y-point and the band gap values obtained in the G_0W_0@LDA+U calculation are equal to 1.21 eV and 1.18 eV for the γ-LiV_2O_5 and γ-NaV_2O_5 structures, respectively. Calculations using U obtained by the linear response method results in E_g values slightly greater (by 0.1 eV) than those computed with the generic U (Table S3).

In the absence of any experimental data concerning the band gap in these materials, we attempt to estimate this quantity by using the Raman and photoluminescence spectroscopies. Note that the above theoretical E_g values imply that the Raman spectra measured using the light sources in the visible region are all obtained in the resonance conditions.

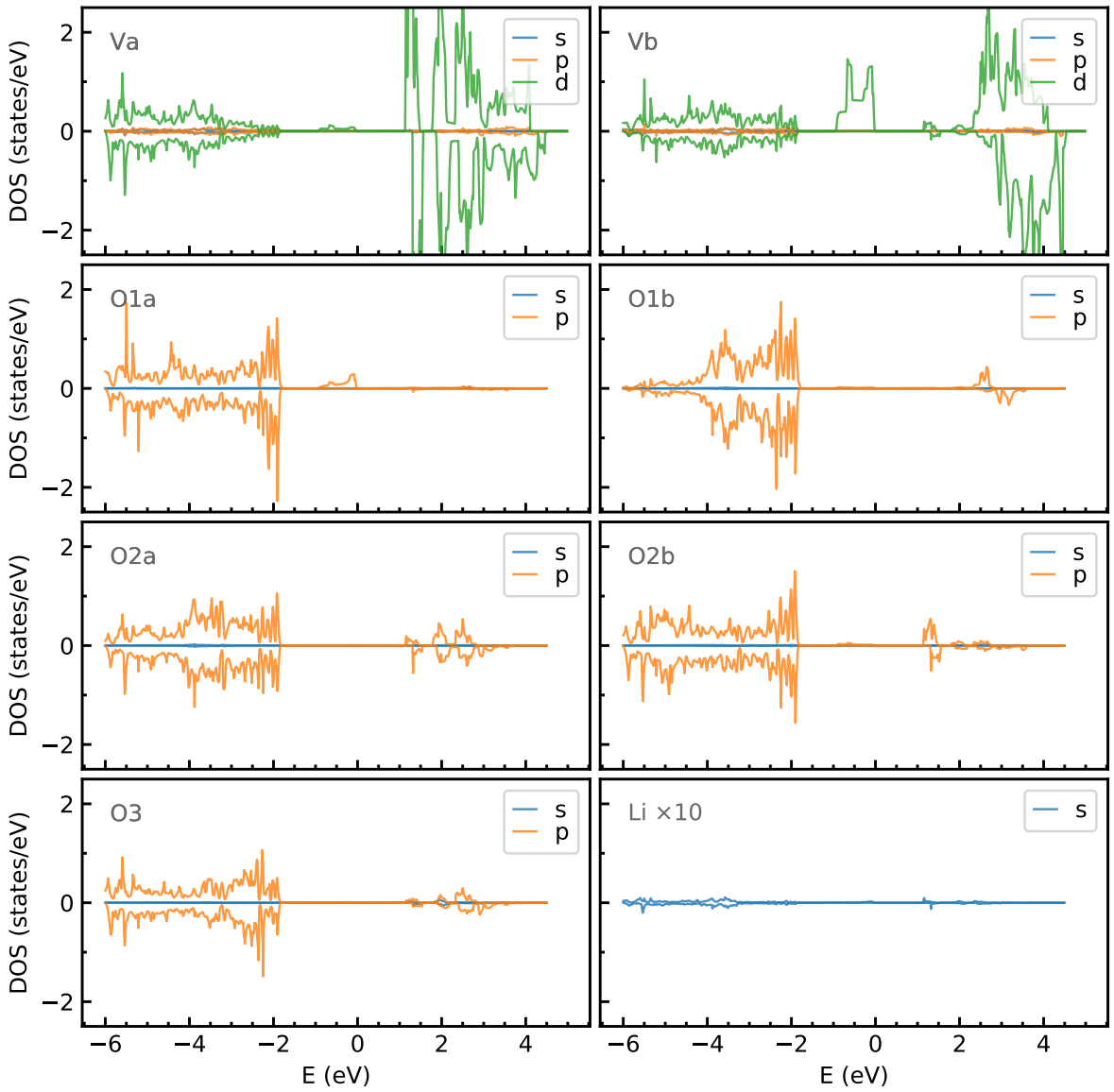

Figure 5: Partial densities of states (PDOS) for γ-LiV_2O_5 obtained in the spin-polarized LDA+U calculation. For each atom type, the positive and negative parts of DOS correspond to the spin up and spin down states. The origin of the energy axis is placed at the Fermi energy.

Figure 5 shows PDOS for the γ-LiV_2O_5 bronze obtained in the spin-polarized LDA+U calculation (see Figure S2 for the total DOS). One readily sees the difference between "spin up" and "spin down" states in the range -0.7 to 0 eV corresponding to the band of localized $3d$ states of Vb atoms. The difference is explained by the fact that with four intercalated Li atoms per unit cell, four electrons ejected from the $2s$ orbitals of lithiums occupy the $3d$ states of Vb atoms in the "spin up" configuration. This leads to the splitting of conduction V^{3d} band to the valence one formed by filled d-states of Vb atom and to the conducting band formed by empty d-states of Va atom (Figure 6). The cation sublattice now consists of vanadium atoms in the 4+ (Vb) and 5+ (Va) oxidation states. This conclusion is in line with the results reported in ref[34] and complete the data in ref[39].

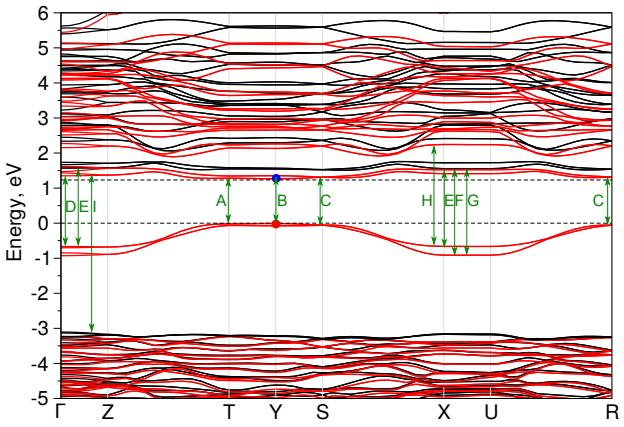

Figure 6: Electron band structure of γ-LiV_2O_5 obtained in G_0W_0@LDA+U calculation. Red and black lines stand for the spin up and spin down states, respectively; dashed lines indicate the positions of the Fermi level and bottom of the conduction band. The bottom of conduction band and the top of the valence band pointed out by blue and red dots respectively. Arrows indicate optical interband transitions, see text for details. The origin of the energy axis is placed at E_F (Fermi energy)

Figure 7 presents the Raman spectra of the γ-LiV_2O_5 bronze measured with the exciting radiation of different wavelengths and the spectrum of γ'-V_2O_5 obtained in off-resonance conditions (corresponding spectra of γ-NaV_2O_5 are given in Figure S4). One sees that peaks in the spectra of γ-LiV_2O_5 are characterized by larger widths and higher intensities compared to the counterpart peaks in the spectrum of the pure compound. It could be supposed that

these peculiarities are due to a more disordered structure of the bronze compared to that of γ'-V_2O_5, however, it is the contrary that should be true. Indeed, γ'-V_2O_5 is obtained by chemical de-intercalation of alkali-metal atoms from γ-LiV_2O_5 and therefore, its resultant structure is expected to contain more defects than that of the parent material. Nevertheless, the peaks in the Raman spectrum of γ'-V_2O_5 shown in Figure 7 are characterized by a notably smaller width. Such a difference between the spectra of the pure and lithiated γ-phases indicates, in our opinion, that the spectra of γ-LiV_2O_5 (and of its sodium analogue) were measured in the electron resonance conditions. If true, this gives an estimation of the band gap in the material $E_g < 1.58$ eV (785 nm) that is in line with the results of the calculations. Unfortunately, all our attempts to obtain the Raman spectra of MeV_2O_5 bronzes with an excitation source of energy smaller than 1.58 eV ($\lambda_0 > 785$ nm) did not succeed due to technical problems.

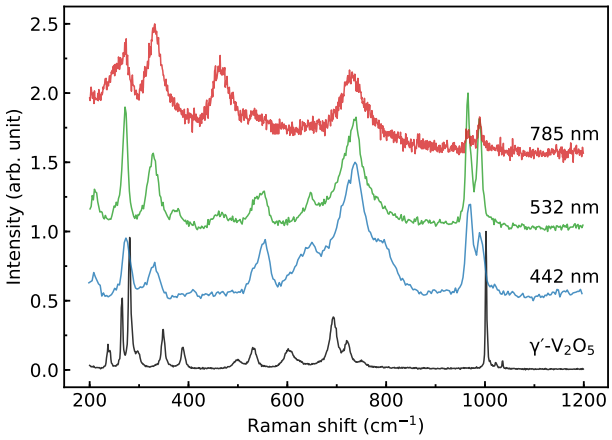

Figure 7: Experimental Raman spectra of γ-LiV_2O_5 measured with the excitation wavelengths $\lambda_0 = 785$ nm (red), $\lambda_0 = 532$ nm (green) and $\lambda_0 = 442$ nm (blue); black line labeled γ'-V_2O_5 presents the experimental Raman spectrum of γ'-V_2O_5 obtained with $\lambda_0 = 633$ nm.

Then, we have attempted to elucidate this issue by using the photoluminescence spectroscopy. Photoluminescence spectra of γ-LiV_2O_5 obtained with different excitation sources are shown in Figure 8 and bands in the spectra are related to specific interband transitions depicted with arrows in Figure 6. The spectrum excited by a low energy radiation, Fig-

ure 8a, has three clear bands labeled A to C that can be related to transitions from the top of the valence band to the bottom of the conduction band in the vicinity of the T, Y, S and R points of the BZ. In the high-energy region, Figure 8b, the bands D and E (Figure 8b) can be associated with transitions in the Γ-point of the BZ and the E, F, G and H bands corresponds to electron transitions at zone boundary points. Finally, the I band may be related to transitions from lower-lying states of the valence zone in the Z-point of the BZ. The calculated electronic structure suggests that the transitions $A-D$ and H occur between states of the same spin, while the transitions $E-G$ and I involve states of different spin.

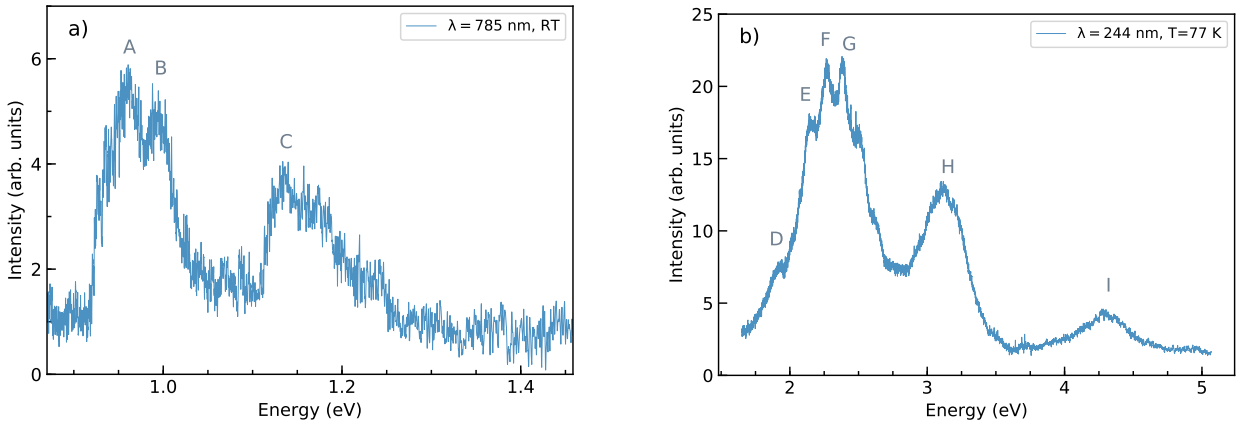

Figure 8: Photoluminescence spectra of γ-LiV_2O_5 sample: a) room temperature (RT), excitation wavelength $\lambda = 785$ nm; b) temperature T = 77 K, excitation wavelength $\lambda = 244$ nm. Letters labeling bands in the spectra refer to transitions depicted in Figure 6.

The energy of the band A, Figure 8a, can be used to estimate the direct band gap value in γ-LiV_2O_5 that gives E_g of *ca.* 0.95 eV at room temperature. Assuming the validity of temperature dependence of E_g in α-V_2O_5 for the bronzes, an approximate band gap at $T = 0$ K in these materials is $E_g \approx 1.15$ eV that reasonably agrees with the value of 1.21 eV obtained in the calculations.

It is noteworthy that all the spectra in Figure 7a-c were measured with the energy of incident radiation smaller than 2.8 eV, *i.e.* the resonance electronic excitation corresponds to the transitions $A-G$, see Figure 6 and Figure 8. These transitions occur between the localized states near the Fermi level formed by the d-orbitals of Vb atoms and the bottom of

the conduction band. This can account for the fact that the most marked difference between the spectra of the γ'-V_2O_5 and γ-LiV_2O_5 samples, Figure 7, is seen for Raman peaks which, according to our calculations, correspond to vibrational modes involving displacements of Vb atoms (see Figure 1).

Conclusions

This work reports results of a combined computational and experimental study of the electronic structure of α-V_2O_5, γ'-V_2O_5 and γ-MeV_2O_5 (Me = Li, Na) materials. The electronic states in these compounds were investigated with the quasi-particle GW method which used a self-consistent LDA+U solution for constructing the initial Green's function and screened Coulomb potential. Such a "single-shot" G_0W_0@LDA+U calculations have given the direct electronic band gap value E_g = 2.89 eV for the α-V_2O_5 structure that well agrees with the available experimental data.[15–17] The strategy was subsequently applied to compute the electronic structure of the γ'-V_2O_5 phase and of the γ-MeV_2O_5 bronzes for which no experimental information on band gap value exists. The calculations have given E_g = 3.17 eV, E_g = 1.21 eV and E_g = 1.18 eV for the γ'-V_2O_5, γ-LiV_2O_5 and γ-NaV_2O_5 structures, respectively. The calculations have shown a close similarity between the electronic structures of the two alkali-atom intercalated materials that accounts for their peculiar and attractive electrochemical characteristicsr.[18] Indeed, while Na insertion systematically occurs at much lower voltage than Li one ($\Delta E \approx 1.5$ V in the case of α-V_2O_5[70]), the same high voltage of 3.3 V *vs.* Na^+/Na is remarkably achieved for Li and Na reactions in γ-MeV_2O_5 bronzes.[18]

The results of electronic-structure calculations were accompanied with data of spectroscopic experiments. Thus, measuring Raman spectra of the materials with different wavelengths of exciting radiation has allowed to estimate a threshold energy corresponding to the transition from off-resonance to resonance Raman scattering process. The band gap value obtained in this way for α-V_2O_5 and γ'-V_2O_5 was found to lie between 2.54 eV and

2.71 eV at room temperature that is in a good agreement with the experimental values for the α-phase and with the result of the G_0W_0@LDA+U calculation. The Raman spectra of γ-MeV_2O_5 bronzes revealed a band gap smaller than 1.58 eV, whereas the comparison of the calculated band structure of γ-LiV_2O_5 with the photoluminescence spectra yielded the band gap $E_g \approx 0.95$ eV for this material. The result of the quasi-particle G_0W_0 calculations is just between the two experimental estimates and is very close to a 0 K value extrapolated from the photoluminescence data. The present work shows that the calculations do not necessitate using adjusted parameters, *i.e.* they can be performed in a fully nonempirical way. The successful approach combining the *ab initio* calculations and spectroscopy will be applied to the investigation of other γ-Me$_x$$V_2O_5$ (Me = K^+, Mg^{2+}, Ca^{2+}, ...) bronzes having a crucial interest for next generation Me-ion batteries.

Supporting Information

Supporting Information is available free of charge on the ACS Publications website at DOI: 10.1021/xxxyyyzzz.

Table with lattice parameters of α-V_2O_5, γ'-V_2O_5, γ-LiV_2O_5 and γ-NaV_2O_5; table with experimental and calculated structural characteristics of γ-LiV_2O_5 and γ-NaV_2O_5; Raman spectra of the α-V_2O_5, γ'-V_2O_5, γ-LiV_2O_5 and γ-NaV_2O_5 materials; electronic band structure and Raman spectra of γ-NaV_2O_5 (PDF).

Author Information

ORCID

Evgenii M. Roginskii: 0000-0002-5627-5877

Mikhail B. Smirnov: 0000-0002-4292-1989

Konstantin S. Smirnov: 0000-0002-8370-8797

Rita Baddour-Hadjean: 0000-0002-3158-1851

Jean-Pierre Pereira-Ramos: 0000-0001-5381-900X

Notes

Authors declare no competing financial interest.

Acknowledgements

E.M.R. acknowledges the financial support of Université Paris Est-Créteil in the frame of the invited professor program UPE 2020. A part of the calculations was performed using the facilities of the Computational Center of Research Park of St. Petersburg State University. The authors also thank the anonymous reviewers for valuable comments.

References

(1) Weckhuysen, B. M.; Keller, D. E. Chemistry, Spectroscopy and the Role of Supported Vanadium Oxides in Heterogeneous Catalysis. *Catal. Today* **2003**, *78*, 25–46, DOI: https://doi.org/10.1016/S0920-5861(02)00323-1.

(2) Chernova, N. A.; Roppolo, M.; Dillon, A. C.; Whittingham, M. S. Layered Vanadium and Molybdenum Oxides: Batteries and Electrochromics. *J. Mater. Chem.* **2009**, *19*, 2526–2552, DOI: https://doi.org/10.1039/B819629J.

(3) Whittingham, M. S. Lithium Batteries and Cathode Materials. *Chem. Rev.* **2004**, *104*, 4271–4301, DOI: 10.1021/cr020731c.

(4) Whittingham, M. S. The Role of Ternary Phases in Cathode Reactions. *J. Electrochem. Soc.* **1976**, *123*, 315–320, DOI: 10.1149/1.2132817.

(5) Delmas, C.; Cognac-Auradou, H.; Cocciantelli, J. M.; Menetrier, M.; Doumerc, J. P. The $Li_xV_2O_5$ System: An Overview of the Structure Modifications Induced by the Lithium Intercalation. *Solid State Ion.* **1994**, *69*, 257–264, DOI: 10.1016/0167-2738(94)90414-6.

(6) Galy, J. Vanadium Pentoxide and Vanadium Oxide Bronzes - Structural Chemistry of Single (S) and Double (D) Layer $M_xV_2O_5$ phases. *J. Solid State Chem.* **1992**, *100*, 229–45, DOI: 10.1016/0022-4596(92)90097-F.

(7) Baddour-Hadjean, R.; Safrany Renard, M.; Pereira-Ramos, J. P. Unraveling the Structural Mechanism of Li Insertion in γ'-V_2O_5 and Its Effect on Cycling Properties. *Acta Mater.* **2019**, *165*, 183–191, DOI: 10.1016/j.actamat.2018.11.043.

(8) Baddour-Hadjean, R.; Safrany Renard, M.; Pereira-Ramos, J. P. Kinetic Insight into the Electrochemical Lithium Insertion Process in the Puckered-Layer γ'-V_2O_5 Polymorph. *J. Electrochem. Soc.* **2019**, *166*, A3474–A3479, DOI: 10.1149/2.1211914jes.

(9) Safrany Renard, M.; Emery, N.; Baddour-Hadjean, R.; Pereira-Ramos, J.-P. γ'-V_2O_5: A New High Voltage Cathode Material for Sodium-Ion Battery. *Electrochim. Acta* **2017**, *252*, 4–11, DOI: 10.1016/j.electacta.2017.08.175.

(10) Baddour-Hadjean, R.; Safrany Renard, M.; Emery, N.; Huynh, L. T. N.; Le, M. L. P.; Pereira-Ramos, J. P. The Richness of V_2O_5 Polymorphs as Superior Cathode Materials for Sodium Insertion. *Electrochim. Acta* **2018**, *270*, 129–137, DOI: 10.1016/j.electacta.2018.03.062.

(11) Zavalij, P. Y.; Whittingham, M. S. Structural Chemistry of Vanadium Oxides with Open Frameworks. *Acta Cryst. B* **1999**, *55*, 627–663, DOI: 10.1107/S0108768199004000.

(12) Eftekhari, A. Lithium-Ion Batteries with High Rate Capabilities. *ACS Sustainable Chem. Eng.* **2017**, *5*, 2799–2816, DOI: 10.1021/acssuschemeng.7b00046.

(13) Bisquert, J.; Cendula, P.; Bertoluzzi, L.; Gimenez, S. Energy Diagram of Semiconductor/Electrolyte Junctions. *J. Phys. Chem. Lett.* **2014**, *5*, 205–207, DOI: 10.1021/jz402703d.

(14) Liu, C.; Neale, Z. G.; Cao, G. Understanding Electrochemical Potentials of Cathode Materials in Rechargeable Batteries. *Mater. Today* **2016**, *19*, 109–123.

(15) Kenny, N.; Kannewurf, C.; Whitmore, D. Optical Absorption Coefficients of Vanadium Pentoxide Single Crystals. *J. Phys. Chem. Solids* **1966**, *27*, 1237 – 1246, DOI: https://doi.org/10.1016/0022-3697(66)90007-2.

(16) Bodó, Z.; Hevesi, I. Optical Absorption near the Absorption Edge in V_2O_5 Single Crystals. *Phys. Status Solidi* **1967**, *20*, K45–K49, DOI: 10.1002/pssb.19670200153.

(17) Meyer, J.; Zilberberg, K.; Riedl, T.; Kahn, A. Electronic Structure of Vanadium Pentoxide: An Efficient Hole Injector for Organic Electronic Materials. *J. Appl. Phys.* **2011**, *110*, 033710, DOI: 10.1063/1.3611392.

(18) Emery, N.; Baddour-Hadjean, R.; Batyrbekuly, D.; Laïk, B.; Bakenov, Z.; Pereira-Ramos, J.-P. γ-$Na_{0.96}V_2O_5$: A New Competitive Cathode Material for Sodium-Ion Batteries Synthesized by a Soft Chemistry Route. *Chem. Mater.* **2018**, *30*, 5305–5314, DOI: 10.1021/acs.chemmater.8b02066.

(19) Perdew, J. P. Density Functional Theory and The Band Gap Problem. *Int. J. Quantum Chem.* **2009**, *28*, 497–523, DOI: 10.1002/qua.560280846.

(20) Mori-Sánchez, P.; Cohen, A. J.; Yang, W. Localization and Delocalization Errors in Density Functional Theory and Implications for Band-Gap Prediction. *Phys. Rev. Lett.* **2008**, *100*, DOI: 10.1103/physrevlett.100.146401.

(21) Anisimov, V. I.; Solovyev, I. V.; Korotin, M. A.; Czyżyk, M. T.; Sawatzky, G. A.

Density Functional Theory and NiO Photoemission Spectra. *Phys. Rev. B* **1993**, *48*, 16929–16934, DOI: 10.1103/PhysRevB.48.16929.

(22) Perdew, J. P.; Ernzerhof, M.; Burke, K. Rationale for Mixing Exact Exchange with Density Functional Approximations. *J. Chem. Phys.* **1996**, *105*, 9982–9985, DOI: 10.1063/1.472933.

(23) Heyd, J.; Scuseria, G. E.; Ernzerhof, M. Hybrid Functionals Based on a Screened Coulomb Potential. *J. Chem. Phys.* **2003**, *118*, 8207–8215, DOI: 10.1063/1.1564060.

(24) Heyd, J.; Scuseria, G. E.; Ernzerhof, M. Erratum: "Hybrid Functionals Based on a Screened Coulomb Potential" [J. Chem. Phys. 118, 8207 (2003)]. *J. Chem. Phys.* **2006**, *124*, 219906, DOI: 10.1063/1.2204597.

(25) Shishkin, M.; Kresse, G. Self-Consistent GW Calculations for Semiconductors and Insulators. *Phys. Rev. B* **2007**, *75*, 235102, DOI: 10.1103/physrevb.75.235102.

(26) Hedin, L. New Method for Calculating the One-Particle Green's Function with Application to the Electron-Gas Problem. *Phys. Rev. A* **1965**, *139*, 796, DOI: https://doi.org/10.1103/PhysRev.139.A796.

(27) Bruneval, F.; Marques, M. A. L. Benchmarking the Starting Points of the GW Approximation for Molecules. *J. Chem. Theory Comput.* **2012**, *9*, 324–329, DOI: 10.1021/ct300835h.

(28) Jiang, H.; Gomez-Abal, R. I.; Rinke, P.; Scheffler, M. Localized and Itinerant States in Lanthanide Oxides United by GW@LDA+U. *Phys. Rev. Lett.* **2009**, *102*, DOI: 10.1103/physrevlett.102.126403.

(29) Jiang, H.; Gomez-Abal, R. I.; Rinke, P.; Scheffler, M. First-Principles Modeling of Localized d States with the GW@LDA+U Approach. *Phys. Rev. B* **2010**, *82*, DOI: 10.1103/physrevb.82.045108.

(30) Kempf, J. Y.; Silvi, B.; Dietrich, A.; Catlow, C. R. A.; Maigret, B. Theoretical Investigations of the Electronic Properties of Vanadium Oxides. 1. Pseudopotential Periodic Hartree-Fock Study of Vanadium Pentoxide Crystal Lattice. *Chem. Mater.* **1993**, *5*, 641–647, DOI: 10.1021/cm00029a011.

(31) Eyert, V.; Höck, K.-H. Electronic Structure of V_2O_5: Role of Octahedral Deformations. *Phys. Rev. B* **1998**, *57*, 12727–12737, DOI: 10.1103/PhysRevB.57.12727.

(32) Willinger, M.; Pinna, N.; Su, D. S.; Schlögl, R. Geometric and Electronic Structure of γ-V_2O_5: Comparison Between α-V_2O_5 and γ-V_2O_5. *Phys. Rev. B* **2004**, *69*, 155114, DOI: https://doi.org/10.1103/PhysRevB.69.155114.

(33) Brázdová, V.; Ganduglia-Pirovano, M. V.; Sauer, J. Periodic Density Functional Study on Structural and Vibrational Properties of Vanadium Oxide Aggregates. *Phys. Rev. B* **2004**, *69*, 165420, DOI: 10.1103/PhysRevB.69.165420.

(34) Scanlon, D. O.; Walsh, A.; Morgan, B. J.; Watson, G. W. An ab initio Study of Reduction of V_2O_5 through the Formation of Oxygen Vacancies and Li Intercalation. *J. Phys. Chem. C* **2008**, *112*, 9903–9911, DOI: https://doi.org/10.1021/jp711334f.

(35) Londero, E.; Schröder, E. Role of van der Waals Bonding in the Layered Oxide V_2O_5: First-principles Density-functional Calculations. *Phys. Rev. B* **2010**, *82*, 054116, DOI: 10.1103/PhysRevB.82.054116.

(36) Londero, E.; Schröder, E. Vanadium Pentoxide (V_2O_5): A van der Waals Density Functional Study. *Comput. Phys. Commun.* **2011**, *182*, 1805 – 1809, DOI: https://doi.org/10.1016/j.cpc.2010.12.036.

(37) Carrasco, J. Role of van der Waals Forces in Thermodynamics and Kinetics of Layered Transition Metal Oxide Electrodes: Alkali and Alkaline-Earth Ion Insertion into V_2O_5. *J. Phys. Chem. C* **2014**, *118*, 19599–19607, DOI: https://doi.org/10.1021/jp505821w.

(38) Zhou, B.; He, D. Raman Spectrum of Vanadium Pentoxide from Density-Functional Perturbation Theory. *J. Raman Spectrosc.* **2008**, *39*, 1475–1481, DOI: 10.1002/jrs.2025.

(39) Smirnov, M. B.; Roginskii, E.; Kazimirov, V. Y.; Smirnov, K. S.; Baddour-Hadjean, R.; Pereira-Ramos, J.-P.; Zhandun, V. Spectroscopic and Computational Study of Structural Changes in γ-LiV_2O_5 Cathodic Material Induced by Lithium Intercalation. *J. Phys. Chem. C* **2015**, *119*, 20801–20809, DOI: 10.1021/acs.jpcc.5b05540.

(40) Bhandari, C.; Lambrecht, W. R. L.; van Schilfgaarde, M. Quasiparticle Self-Consistent GW Calculations of the Electronic Band Structure of Bulk and Monolayer V_2O_5. *Phys. Rev. B* **2015**, *91*, 125116, DOI: 10.1103/physrevb.91.125116.

(41) Cococcioni, M.; de Gironcoli, S. Linear Response Approach to the Calculation of the Effective Interaction Parameters in the LDA + U Method. *Phys. Rev. B* **2005**, *71*, 035105, DOI: 10.1103/PhysRevB.71.035105.

(42) Mjejri, I.; Rougier, A.; Gaudon, M. Low-Cost and Facile Synthesis of the Vanadium Oxides V_2O_3, VO_2, and V_2O_5 and Their Magnetic, Thermochromic and Electrochromic Properties. *Inorg. Chem.* **2017**, *56*, 1734–1741, DOI: 10.1021/acs.inorgchem.6b02880.

(43) Murphy, D. W.; Christian, P. A.; DiSalvo, F. J.; Waszczak, J. V. Lithium Incorporation by Vanadium Pentoxide. *Inorg. Chem.* **1979**, *18*, 2800–2803, DOI: 10.1021/ic50200a034.

(44) Baddour-Hadjean, R.; Smirnov, M. B.; Kazimirov, V. Y.; Smirnov, K. S.; Pereira-Ramos, J.-P. The Raman Spectrum of the γ'-V_2O_5 Polymorph: A Combined Experimental and DFT Study. *J. Raman Spectrosc.* **2015**, *46*, 406–412, DOI: 10.1002/jrs.4660.

(45) Safrany Renard, M.; Emery, N.; Roginskii, E. M.; Baddour-Hadjean, R.; Pereira-Ramos, J. P. Crystal Structure Determination of a New Sodium Vanadium Bronze Electrochemically Formed. *J. Solid State Chem.* **2017**, *254*, 62–68, DOI: 10.1016/j.jssc.2017.07.012.

(46) Smirnov, M. B.; Roginskii, E. M.; Smirnov, K. S.; Baddour-Hadjean, R.; Pereira-Ramos, J.-P. Unraveling the Structure-Raman Spectra Relationships in V_2O_5 Polymorphs via a Comprehensive Experimental and DFT Study. *Inorg. Chem.* **2018**, *57*, 9190–9204, DOI: 10.1021/acs.inorgchem.8b01212.

(47) Gonze, X. et al. ABINIT: First-Principles Approach to Material and Nanosystem Properties. *Comput. Phys. Commun.* **2009**, *180*, 2582–2615, DOI: https://doi.org/10.1016/j.cpc.2009.07.007.

(48) Gonze, X. et al. A Brief Introduction to the ABINIT Software Package. *Z. Kristallogr. Cryst. Mater.* **2005**, *220*, 558–562, DOI: 10.1524/zkri.220.5.558.65066.

(49) Perdew, J. P.; Wang, Y. Accurate and Simple Analytic Representation of the Electron-Gas Correlation Energy. *Phy. Rev. B* **1992**, *45*, 13244–13249, DOI: 10.1103/physrevb.45.13244.

(50) Blöchl, P. E. Projector Augmented-Wave Method. *Phys. Rev. B* **1994**, *50*, 17953–17979, DOI: https://doi.org/10.1103/PhysRevB.50.17953.

(51) Kresse, G.; Joubert, D. From Ultrasoft Pseudopotentials to the Projector Augmented-Wave Method. *Phys. Rev. B* **1999**, *59*, 1758–1775, DOI: https://doi.org/10.1103/PhysRevB.59.1758.

(52) Murnaghan, F. D. The Compressibility of Media under Extreme Pressures. *PNAS* **1944**, *30*, 244–247, DOI: https://doi.org/10.1073/pnas.30.9.244.

(53) Monkhorst, H. J.; Pack, J. D. Special Points for Brillouin-Zone Integrations. *Phys. Rev. B* **1976**, *13*, 5188–5192, DOI: https://doi.org/10.1103/PhysRevB.13.5188.

(54) Aulbur, W. G.; Jönsson, L.; Wilkins, J. W. *Solid State Phys.*; Academic Press, 2000; Vol. 54; pp 1–218.

(55) Lebègue, S.; Arnaud, B.; Alouani, M.; Bloechl, P. E. Implementation of an All-Electron GW Approximation Based on the Projector Augmented Wave Method Without Plasmon Pole Approximation: Application to Si, SiC, AlAs, InAs, NaH, and KH. *Phys. Rev. B* **2003**, *67*, DOI: 10.1103/physrevb.67.155208.

(56) Patrick, C. E.; Giustino, F. GW Quasiparticle Bandgaps of Anatase TiO_2 Starting from DFT + U. *J. Phys. Condens. Matter* **2012**, *24*, 202201, DOI: 10.1088/0953-8984/24/20/202201.

(57) Himmetoglu, B.; Floris, A.; de Gironcoli, S.; Cococcioni, M. Hubbard-Corrected DFT Energy Functionals: the LDA+U Description of Correlated Systems. *Int. J. Quantum Chem.* **2013**, *114*, 14–49, DOI: DOI:␣10.1002/qua.24521.

(58) Levine, Z. H.; Allan, D. C. Linear Optical Response in Silicon and Germanium Including Self-Energy Effects. *Phys. Rev. Lett.* **1989**, *63*, 1719–1722, DOI: 10.1103/physrevlett.63.1719.

(59) The official github mirror of the ABINIT repository.

(60) Wu Q. H., J. W., Thissen A. Photoelectron Spectroscopic Study of Li Intercalation into V_2O_5 Thin Films. *Surf. Sci.* **2005**, *578*, 203–212, DOI: 10.1016/j.susc.2005.01.042.

(61) Wu Q. H., J. W., Thissen A. Photoelectron Spectroscopic Study of Na Intercalation into V_2O_5 Thin Films. *Solid State Ion.* **2004**, *167*, 155–163, DOI: 10.1016/j.ssi.2003.12.016.

(62) Shick, A. B.; Liechtenstein, A. I.; Pickett, W. E. Implementation of the LDA+U Method Using the Full-Potential Linearized Augmented Plane-Wave Basis. *Phys. Rev. B* **1999**, *60*, 10763–10769, DOI: 10.1103/physrevb.60.10763.

(63) Bennett, J. W.; Hudson, B. G.; Metz, I. K.; Liang, D.; Spurgeon, S.; Cui, Q.; Mason, S. E. A Systematic Determination of Hubbard U Using the GBRV Ultrasoft Pseudopotential Set. *Comput. Mater. Sci.* **2019**, *170*, 109137, DOI: 10.1016/j.commatsci.2019.109137.

(64) Porsev, V. V.; Bandura, A. V.; Evarestov, R. A. Hybrid Hartree-Fock-Density Functional Theory Study of V_2O_5 Three Phases: Comparison of Bulk and Layer Stability, Electron and Phonon Properties. *Acta Materialia* **2014**, *75*, 246 – 258, DOI: https://doi.org/10.1016/j.actamat.2014.04.068.

(65) Carrier, P.; Rohra, S.; Görling, A. General Treatment of the Singularities in Hartree-Fock and Exact-Exchange Kohn-Sham Methods for Solids. *Phys. Rev. B* **2007**, *75*, 205126, DOI: 10.1103/PhysRevB.75.205126.

(66) Wang, L.; Maxisch, T.; Ceder, G. Oxidation Energies of Transition Metal Oxides within the GGA + U Framework. *Phys. Rev. B* **2006**, *73*, 195107, DOI: 10.1103/PhysRevB.73.195107.

(67) Da Silva, J. L. F.; Ganduglia-Pirovano, M. V.; Sauer, J. Formation of the Cerium Orthovanadate $CeVO_4$: DFT + U Study. *Phys. Rev. B* **2007**, *76*, 125117, DOI: 10.1103/PhysRevB.76.125117.

(68) Goclon, J.; Grybos, R.; Witko, M.; Hafner, J. Relative Stability of Low-Index V_2O_5surfaces: A Density Dunctional Investigation. *J. Phys.: Condens. Matter* **2009**, *21*, 095008, DOI: 10.1088/0953-8984/21/9/095008.

(69) Gallardo-Amores, J. M.; Biskup, N.; Amador, U.; Persson, K.; Ceder, G.; Morán, E.; Arroyo y de Dompablo, M. E. Computational and Experimental Investigation of the

Transformation of V_2O_5 Under Pressure. *Chem. Mater.* **2007**, *19*, 5262–5271, DOI: 10.1021/cm071360p.

(70) Muller-Bouvet, D.; Baddour-Hadjean, R.; Tanabe, M.; Huynh, L.; Le, M.; Pereira-Ramos, J. Electrochemically Formed α'-NaV_2O_5: A New Sodium Intercalation Compound. *Electrochim. Acta* **2015**, *176*, 586 – 593, DOI: https://doi.org/10.1016/j.electacta.2015.07.030.